# A mm-Wave Wideband/Reconfigurable LNA Using a 3-Winding Transformer Load in 22-nm CMOS FDSOI

Mohammad Ghaedi Bardeh, Jierui Fu, Navid Naseh, Jeyanandh Paramesh, Kamran Entesari Electrical and Computer Engineering, Texas A&M University, USA {m.ghaedi95, jierui.fu, nnaseh, kentesar}@tamu.edu, jeyanandh.paramesh@ieee.org

Abstract - A mm-Wave wideband/reconfigurable LNA using a 3-winding transformer load has been implemented in 22-nm CMOS FDSOI technology for 5G applications. The proposed LNA has three stages with the first two stages utilizing a novel 3-winding transformer as a load to provide three parallel paths, one main and two auxiliary paths. The load expands the frequency band of interest in the wideband mode when the main path is active and reconfigures the LNA bandwidth in the reconfigurable mode when either of the auxiliary paths are active. The third stage acts as a buffer. The LNA shows a measured S21 by the peak gain of 32 at 30 GHz and 3-dB bandwidth of 12.6 GHz for the wideband mode and peak gains of 32.4 dB and 33.4 dB at 22 and 29 GHz for 3-dB bandwidths of 5 and 5.3 GHz for two auxiliary paths in the reconfigurable mode, respectively. The measured NF is lower than 4.5 dB for the entire frequency band and measured OP1dB and OIP3 are better than -6 dBm and 2 dBm for the entire frequency band of interest, respectively. The total power consumption of the proposed LNA is 35 mW in each mode of working, and the chip area is 1155  $\mu$ m imes 642  $\mu$ m excluding pads.

Keywords — mm-wave LNA, reconfigurable, wide-band, 3-winding transformer, double-tuned transformer.

## I. INTRODUCTION

The demand for having higher data rates communication systems has derived the motivation of moving forward from RF frequency operation to mm-Wave frequencies. In mm-Wave frequency bands, the free space path loss is much higher than lower frequencies [1], [2]. To mitigate the high path loss problem in mm-wave systems, multiple-input multiple-output (MIMO) techniques are extensively used.

One of the key elements of a MIMO system front-end (FE) channel is the low-noise amplifier (LNA). Having wide bandwidth, low noise performance, low power consumption, and high linearity are the main challenges of designing an LNA that covers 5G frequency band of operation. To cover the frequency band requirement for 5G applications, several approaches are introduced that are categorized as wideband and reconfigurable. Using source-gate feedback and inductor peaking in [3], [4], gate-drain mutually induced feedback in [5], double-tuned transformers in [6], and one-port coupled resonator as load in [7], [8] are the techniques that are reported in recent state-of-the-art wideband LNAs. Another approach to realize mm-Wave LNAs is using reconfigurable techniques. There are several different approaches that can be used to design mm-Wave frequency reconfigurable LNAs. In [9], a reconfigurable LNA for 28/60 GHz is presented using an extra inductor controlled by a switch. By turning the switch OFF

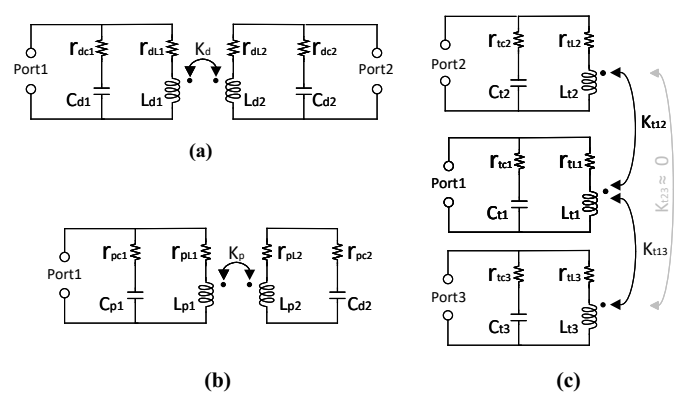


Fig. 1. Different coupled transformers as resonance load. (a) Double-tuned. (b) One-port double-tuned. (c) The proposed 3-winding transformer.

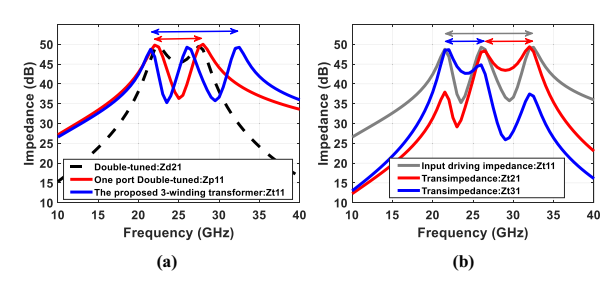


Fig. 2. (a) Frequency response comparison of three transformers. (b) Frequency response of the proposed 3-winding transformer in different modes.

and ON, the frequency changes from 28 to 60 GHz. The drawback here is limiting the inductor Q while switching its value directly at mm-Wave range. In [10], by using a variable inductor based on open and ground shielding area around the inductor another mm-Wave reconfigurable LNA is presented where the drawback is the complexity of providing effective ground in the LNA layout. One main challenge in designing reconfigurable mm-Wave LNAs is having equal specifications for LNA in different bands in terms of S21, NF, power consumption, and linearity. Another major challenge is that switching is done at mm-Wave frequencies where on-resistance and off-capacitance of the switch limit the S21 performance.

To address the aforementioned issues, a mm-Wave wide-band (21.6-34.2GHz)/ reconfigurable LNA is presented in this paper that uses a novel 3-winding transformer as a resonance load to enable three different frequency modes:

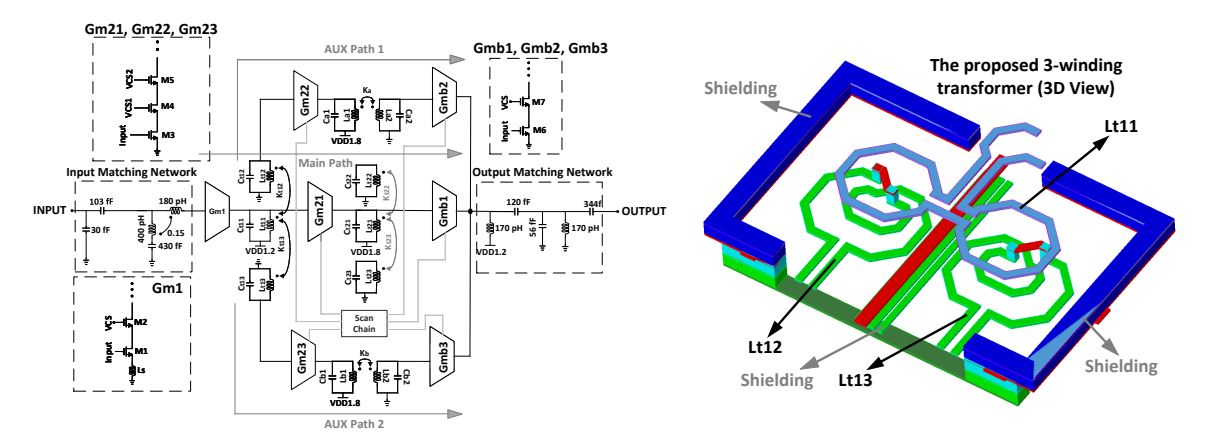


Fig. 3. Block diagram of the proposed LNA(left) and 3D layout of the 3-winding transformer (right).

1) Wide-band (21.6-34.2 GHz) frequency operation, 2) Low frequency (21.5-26.5 GHz) operation, and 3) High frequency (27.5-33 GHz) operation. Therefore, the proposed mm-Wave LNA with the frequency band of operation of 21.6-34.2 GHz, peak S21 of 32 at 30 GHz, NF of < 4.5 dB for 21.6-34.2 GHz, and S11 and S22 < -10 dB for the entire frequency band of interest have advantageous of both (wideband and reconfigurable) LNAs. One reason to move from wide-band operation to the reconfigurable one is to increase out-of-band IIP3 to handle interferers which are common in MIMO phased array systems.

# II. 3-WINDING TRANSFORMER TOPOLOGY

Double-tuned transformers are a popular choice as wideband resonance loads for mm-wave LNAs to extend the operating frequency of the LNA. Traditionally, to achieve a wide-band load, the transimpedance parameter  $(Z_{21})$  is used in a double-tuned transformer (Fig. 1(a)). But, as shown in Fig. 1(b), the input driving point  $(Z_{11})$  can potentially have higher gain-bandwidth (GBW) compared to transimpedance  $(Z_{21})$  as  $Z_{11}$  has an additional complex-conjugate zero pair that helps to increase the bandwidth of  $Z_{11}$  compared to  $Z_{21}$  [7]. Having inspired by this fact and the need to have both wide-band and reconfigurable LNAs to take advantage of both modes, a novel 3-winding transformer is presented that can simultaneously achieve reconfigurability, and wide bandwidth as shown in Fig. 1(c) which three ports (1, 2, and 3) can be used to achieve different operating frequency band. The proposed structure in Fig. 1(c) has one more inductor compared to two structures in Fig. 1(a), (b), which means having one pair of poles, therefore; it will have wider bandwidth compared to the conventional double-tuned transformer. The transformer is designed such that the coupling coefficient from the primary to each secondary is low, yet well controlled (e.g,  $k_{12} = k_{13} = 0.21$ ), but the secondaries have negligible mutual coupling (i.e.,  $k_{23} \cong 0$ ). The resonators can be designed to have equal un-coupled resonant frequencies, but magnetic coupling causes pole-splitting action resulting in a wideband response. Fig. 2(a) shows the frequency response comparison between three cases: 1) Transimpedance  $(Z_{d21})$ 

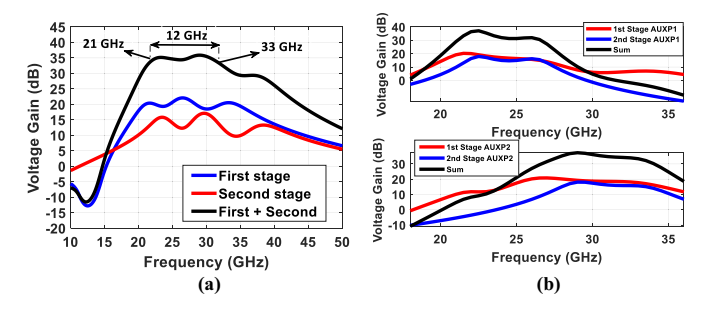


Fig. 4. (a) Simulated small signal voltage gain of the first and second stage in wide-band mode (ripple compensation). (b) low- frequency and high-frequency reconfigurable modes.

of a conventional double-tuned transformer, 2) Input driving impedance  $(Z_{p11})$  of a conventional double-tuned transformer, and 3) Input driving impedance  $(Z_{t11})$  of the proposed 3-winding transformer. As can be seen, for roughly equal values of inductors and coupling factors in three scenarios,  $Z_{t11}$  has higher frequency of operation ( $\approx 4$  GHz) compared to other approaches. Also, Fig. 2(b) shows the frequency response for  $Z_{t11}$ ,  $Z_{t21}$ , and  $Z_{t31}$ , where  $Z_{t11}$  mode covers entire frequency band,  $Z_{t21}$  supports lower frequency band, and  $Z_{t31}$ supports higher frequency band of operation.  $Z_{t11}$  response can be tailored to achieve wide bandwidth with low ripple, but with gradual stop-band skirts.  $Z_{t21}$  and  $Z_{t31}$  responses have lower ripple, but with lower bandwidth and sharper stop-band skirts. This load is used in the proposed LNA to reconfigure between these responses and trade bandwidth for out-of-band linearity.

#### III. LNA DESIGN

# A. System-Level Architecture

The block diagram of the proposed mm-Wave wideband/reconfigurable LNA is shown in Fig. 3. The circuit employs three gain stages. The first stage starts with an input matching network to provide proper power transmission in the frequency band of interest. After the input matching network, there is the first  $G_m$  cell that amplifies the signal through the first stage of the proposed 3-winding transformer. At this stage, there are three possible

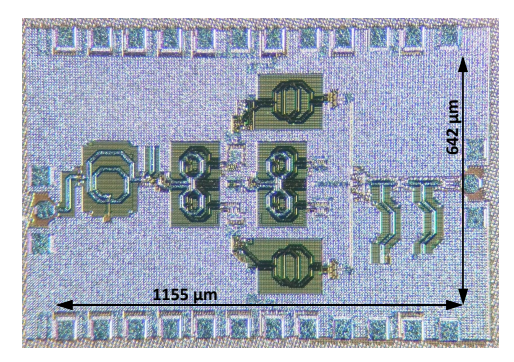


Fig. 5. Chip photograph of the proposed LNA.

paths for the signal, the main path in the middle marked as 'Main Path', and the two auxiliary paths marked as 'Aux Path1' and 'Aux Path 2' in Fig. 3. Then, the auxiliary paths (reconfigurable modes) each employ a  $G_m$  cell and a conventional double-tuned transformer to adjust the amplified signal to have a flat response in low and high frequency bands. The middle path is the main path where the signal is amplified and adjusted through the second stage of the proposed 3-winding transformer to have acceptable gain and flatness in the whole frequency band of operation. The selection of the function of the LNA between the three modes is done through the scan chain by turning on proper  $G_{m2i}$  and  $G_{mbi}(i=1,2,3)$  transconductance cells in Fig. 3. Finally, the signals are fed into a combiner that is consisted of three parallel  $G_m$  cells  $(G_{mbi}(i=1,2,3))$  where each one is ON depending on the selected mode. The buffer stage  $G_m$ cells  $(G_{mb1}, G_{mb2}, G_{mb3})$  are designed in a cascode manner and all three parallel output paths of  $G_m$  cells are combined together and connected to the output matching network. Also, the capacitors  $C_{t1i}$  and  $C_{t2i}$  (i = 1, 2, 3) are tunable MOM capacitors which are optimized to provide maximum quality factor.

## B. Circuit Design

The first stage consists of a cascode common-source (CS) with source degeneration including M1 and M2 which are biased and the layout of two transistors are customized to provide minimum NF over the entire frequency band of operation [11]. To compensate for the ripples out of the first 3-winding transformer, the second stage is designed to ensure gain flatness of all three parallel paths by skewing the pole positions of  $Z_{t11}$  the second 3-winding transformer in the main path compared to the  $Z_{t11}$  of the first 3-winding transformer and by properly locating the poles of  $Z_{d21}$  of the double-tuned transformers in both upper and lower paths. To ensure better isolation between the first and second stages, a triple-stacked structure is used in the  $G_m$  cells of the second stage  $(G_{m21}, G_{m22}, G_{m23})$ . Fig. 4(a) shows the simulated voltage gain of each stage and also the total voltage gain for the wideband mode when the main path is active. Also, Fig. 4(b) top and bottom show the simulated voltage gain for auxiliary paths 1 and 2 (low- and high-frequency modes), respectively.

Table 1. Performance comparison with the state of the art mm-wave LNAs

Ref.	Freq.	Peak	Min	Туре	Min	Power
&	(GHz)	Gain	NF		OP1dB	(mW)
Tech.		(dB)	(dB)		(dBm)	
This	21.6-34.2	32	2.3	$\mathbf{WB}^1$	-6	35@1.2/1.8
work	21.5-26.5	32.4	2.7	$RC^2$	-7	35@1.2/1.8
22 FDSOI	27.5-33	33.4	2.3	$RC^2$	-6.2	35@1.2/1.8
[11]	23.7-30.3	22	2.55	CC <sup>3</sup>	-10.5 <sup>4</sup>	18
22 FDSOI	38-42.7	16			-7	@0.8/1
[7]	24.4-32.3	24.4	4	$WB^1$	0.4	22
65 CMOS						@1.1
[9]	28/60	16.2	2.8	$RC^2$	3.2	8.2
130 SiGe		15	3.35		7	21
[4]	24-43	23	3.1	$WB^1$	-4	20.5
22 FDSOI						@1/1.6
[3]	19-36	21.5	1.7	$WB^1$	-	17.03
22 FDSOI						@1.05
[10]	24/38	9.5/12	4.5	$RC^2$	-3.5	20.28
45 SOI	/39	/15.5			-4.1	@1.5

 $<sup>^1</sup>$  WB = Wideband.  $^2$  RC = Reconfigurable.  $^3$  CC = Concurrent.  $^4$  Approximated as  $(Gain_{dB}-1)+iP_{1dB}$  when measurement result not available.

The supply voltage for the first, second, and buffer stages are 1.2 v and 1.8 v, and 1.2, and the current consumptions are 12 mA, 8 mA (each of the three parallel paths in the second stage consumes 8 mA but only one of which is ON at a time), and 10 mA respectively.

# C. Input/Output Matching Circuits

The input matching circuit is designed to provide one zero in low frequency (around 12 GHz) to ensure filtering unwanted low frequency out-of-band interference and has two poles at 24 and 28 GHz where their location is determined by the coupling factor of the two inductors (180 pH and 400 pH) set ot be  $\sim 0.15$ . Also, to ensure maximum power transfer at the output, a second order output matching network with two poles at 23 and 34 GHz is designed to ensure S22 < -10 dB for the entire frequency band of interest.

# IV. MEASUREMENT RESULTS

The proposed mm-wave wideband/reconfigurable LNA is fabricated in 22-nm CMOS FDSOI technology from Global Foundries with the area of  $1155~\mu m \times 642~\mu m$  (excluding pads). The die photograph is shown in Fig. 5. According to Fig. 5, the chip is measured using dc-probes on top and bottom of the chip for dc-biases and RF-probes for input (left side of the chip) and output (right side of the chip). The effect of probes are de-embedded the using through-open-short-match (TOSM) calibration substrate. The S-parameter, P1dB, and IIP3 are measured using Rohde & Schwarz ZVA67 network analyzer. Also, NF is measured using the Rohde & Schwarz FSV40 spectrum analyzer and Keysight 346CK01 noise source. The proposed LNA consumes 35 mW for both wideband and reconfigurable modes, respectively.

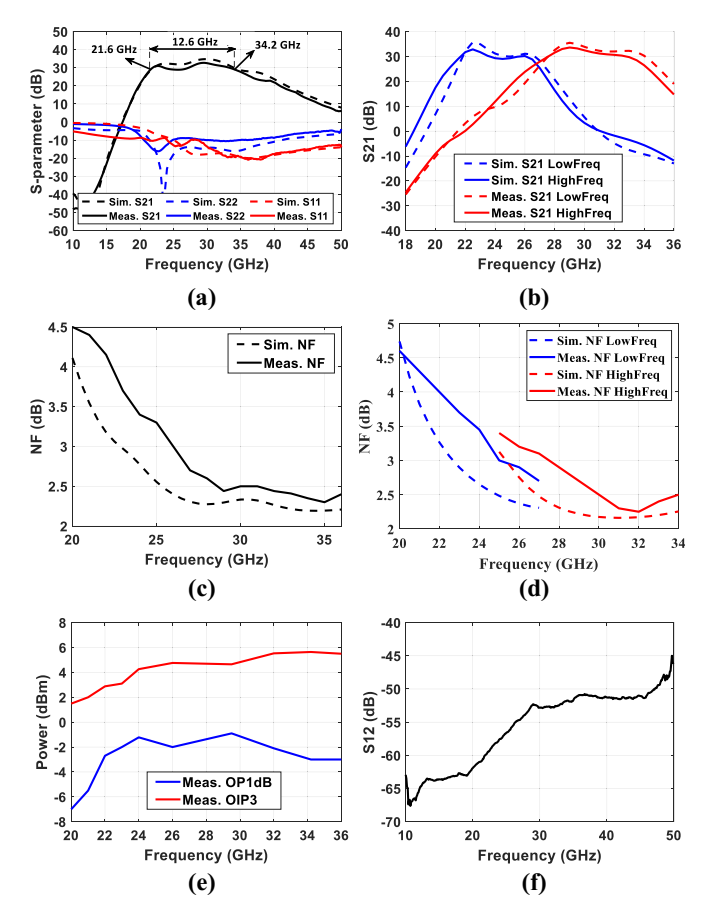


Fig. 6. Measured and simulated results of the proposed LNA. (a) The S-parameter for wideband mode. (b) S21 for reconfigurable mode. (c) Wide-band mode NF. (d) Reconfigurable mode NF. (e) OIP3 and OP1dB for wideband mode. (f) S12 for wideband mode.

Fig. 6(a), (b) show the measured results for S21, S11, and S22 versus frequency for three modes of operation. As shown, the measured 3-dB gain bandwidth of S21 for wide-band mode is from 21.6 to 34.2 GHz with a peak gain of 32 dB at 30 GHz which matches the simulation results of S21. The measured low-frequency mode of S21 is shown in Fig. 6(b) with 3-dB gain bandwidth from 21.5 to 26.5 GHz by the peak gain of 32.4 at 22 GHz. Also, the 3-dB gain bandwidth of the measured high-frequency mode of S21 is from 27.5 to 33 GHz by the peak gain of 34.4 dB at 29 GHz. Both measured S21 values for low-and high-frequency modes are also very close to the simulation results. The measured S11 and S22 are < -10 dB from 20 to 36 GHz which covers the entire frequency band of interest. Also, S11 and S22 for reconfigurable modes are identical to wide-band mode since the first stage is the same. Fig. 6(c), (d) show the measured and simulated NF for both wide-band and reconfigure modes. The minimum measured NF is 2.3 at 35 GHz. Fig. 6(e) shows the OIP3 and OP1dB measurement results of the proposed LNA which the maximum measured OIP3 and OP1dB of -0.9 and 5.8, are achieved. Finally, Fig. 6(f) shows measured S12 < -45 dB for the entire frequency.

The chip performance and comparison with the

state-of-the-art is summarized in Table 1. The proposed LNA in wideband mode has comparable and even better results compared to other wideband LNAs. To our knowledge, this is the first LNA that can work in both wideband and reconfigurable modes.

#### V. CONCLUSION

A mm-Wave wideband/reconfigurable LNA using a 3-winding transformer load has been implemented in 22-nm CMOS FDSOI technology for 5G applications. The LNA shows measured S21 by the peak gain of 32 at 30 GHz and 3-dB bandwidth of 12.6 GHz for wide-band mode and peak gain of 32.4 dB and 34.4 dB for 3-dB bandwidth of 5 and 5.5 GHz using two auxiliary paths for low- and high-frequency modes, respectively. The measured NF is lower than 4.5 dB for the entire band for both modes. The total power consumption of the proposed LNA is 35 mW for both modes of operation.

## ACKNOWLEDGMENT

This project is founded through NSF award No. 2116498. The authors would like to thank Global Foundries for the chip fabrication.

## REFERENCES

- M. G. Bardeh, J. Fu, N. Naseh, J. Paramesh, and K. Entesari, "A wideband low RMS phase/gain error mm-wave phase shifter in 22-nm CMOS FDSOI," *IEEE Microwave and Wireless Technology Letters*, 2023.
- [2] M. G. Bardeh, N. Naseh, J. Fu, J. Paramesh, and K. Entesari, "A mm-wave RC PPF quadrature network with gain boosting in 22nm CMOS FDSOI," in 2023 IEEE Radio and Wireless Symposium (RWS). IEEE, 2023, pp. 108–110.
- [3] B. Cui and J. R. Long, "A 1.7-dB minimum NF, 22–32-GHz low-noise feedback amplifier with multistage noise matching in 22-nm FD-SOI CMOS," *IEEE Journal of Solid-State Circuits*, vol. 55, no. 5, pp. 1239–1248, 2020.
- [4] L. Gao and G. M. Rebeiz, "A 24-43 GHz LNA with 3.1-3.7 dB noise figure and embedded 3-pole elliptic high-pass response for 5G applications in 22 nm FDSOI," in 2019 IEEE Radio Frequency Integrated Circuits Symposium (RFIC). IEEE, 2019, pp. 239–242.
- [5] A. Ershadi, S. Palermo, and K. Entesari, "A 22.2-43 GHz gate-drain mutually induced feedback low noise amplifier in 28-nm CMOS," in 2021 IEEE Radio Frequency Integrated Circuits Symposium (RFIC). IEEE, 2021, pp. 27–30.
- [6] M. Elkholy, S. Shakib, J. Dunworth, V. Aparin, and K. Entesari, "A wideband variable gain LNA with high OIP3 for 5G using 40-nm bulk CMOS," *IEEE Microwave and Wireless Components Letters*, vol. 28, no. 1, pp. 64–66, 2017.
- [7] R. Singh, S. Mondal, and J. Paramesh, "A millimeter-wave receiver using a wideband low-noise amplifier with one-port coupled resonator loads," *IEEE Transactions on Microwave Theory and Techniques*, vol. 68, no. 9, pp. 3794–3803, 2020.
- [8] M. El-Nozahi, E. Sánchez-Sinencio, and K. Entesari, "A millimeter-wave (23–32 GHz) wideband BiCMOS low-noise amplifier," *IEEE Journal of Solid-State Circuits*, vol. 45, no. 2, pp. 289–299, 2010.
- [9] A. A. Nawaz, J. D. Albrecht, and A. Ç. Ulusoy, "A Ka/V band-switchable LNA with 2.8/3.4 dB noise figure," *IEEE Microwave and Wireless Components Letters*, vol. 29, no. 10, pp. 662–664, 2019.
- [10] R. A. Shaheen, T. Rahkonen, and A. Pärssinen, "Millimeter-wave frequency reconfigurable low noise amplifiers for 5G," *IEEE Transactions on Circuits and Systems II: Express Briefs*, vol. 68, no. 2, pp. 642–646, 2020.
- [11] J. Fu, M. G. Bardeh, J. Paramesh, and K. Entesari, "A Millimeter-Wave Concurrent LNA in 22-nm CMOS FDSOI for 5G applications," *IEEE Transactions on Microwave Theory and Techniques*, 2022.